Supplementary Information

Construction of Pnictogen-Rich Cyclophosphazene-Based Manganese(II) Coordination Polymers: Structural Insights and Visible-Light Photocatalytic Activity

Rabia Emir[a], Elif Özcan*[a] and Yunus Zorlu*[a]

[a]Gebze Tehnical University, Chemistry Department, 41400, Gebze-Kocaeli, Türkiye

Table of Contents

Table S8. Selected bond lengths (Å) and bond angles (°) for **PCP-28.**
Table S9. Selected bond lengths (Å) and bond angles (°) for **PCP-29.**
Table S10. Comparison of photocatalytic activity of Mn(II) PCPs from literature and PCPs synthesized in this study.

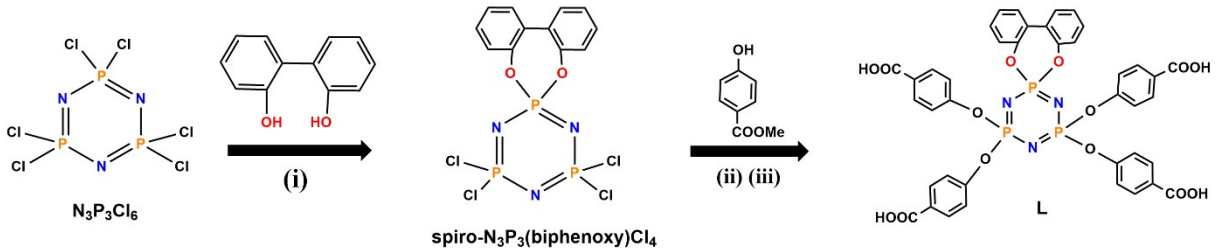

Scheme S1. Synthesis route of **H_4L. i).** K_2CO_3, Acetone, rt; **ii).** K_2CO_3, Acetone,reflux; **iii).** NaOH, MeOH, 80 °C/ pH 2-3 with 0.1 M HCl.

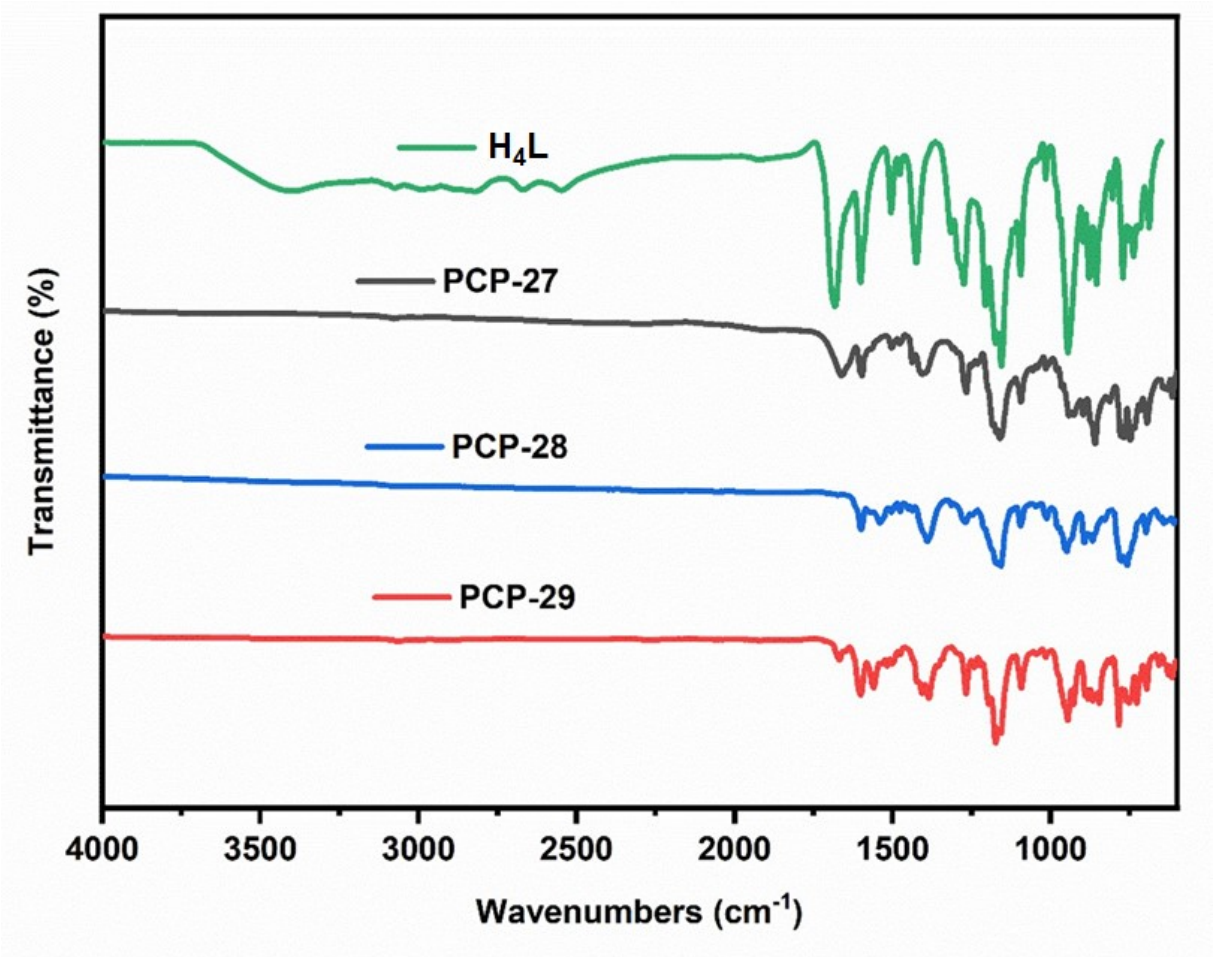

Figure S1. FTIR spectra of **H_4L**, **PCP-27**, **PCP-28**, and **PCP-29**.

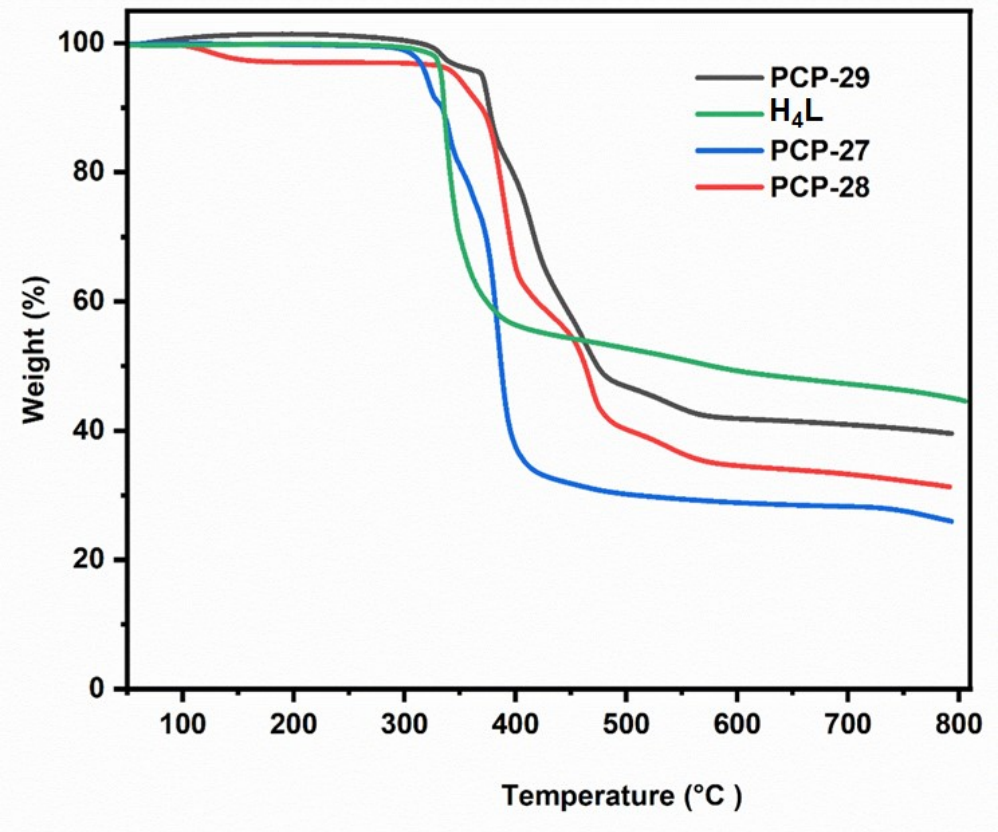

Figure S2. TGA curves of ligand (**H_4L**) and PCPs (**PCP-27, PCP-28, PCP-29**).

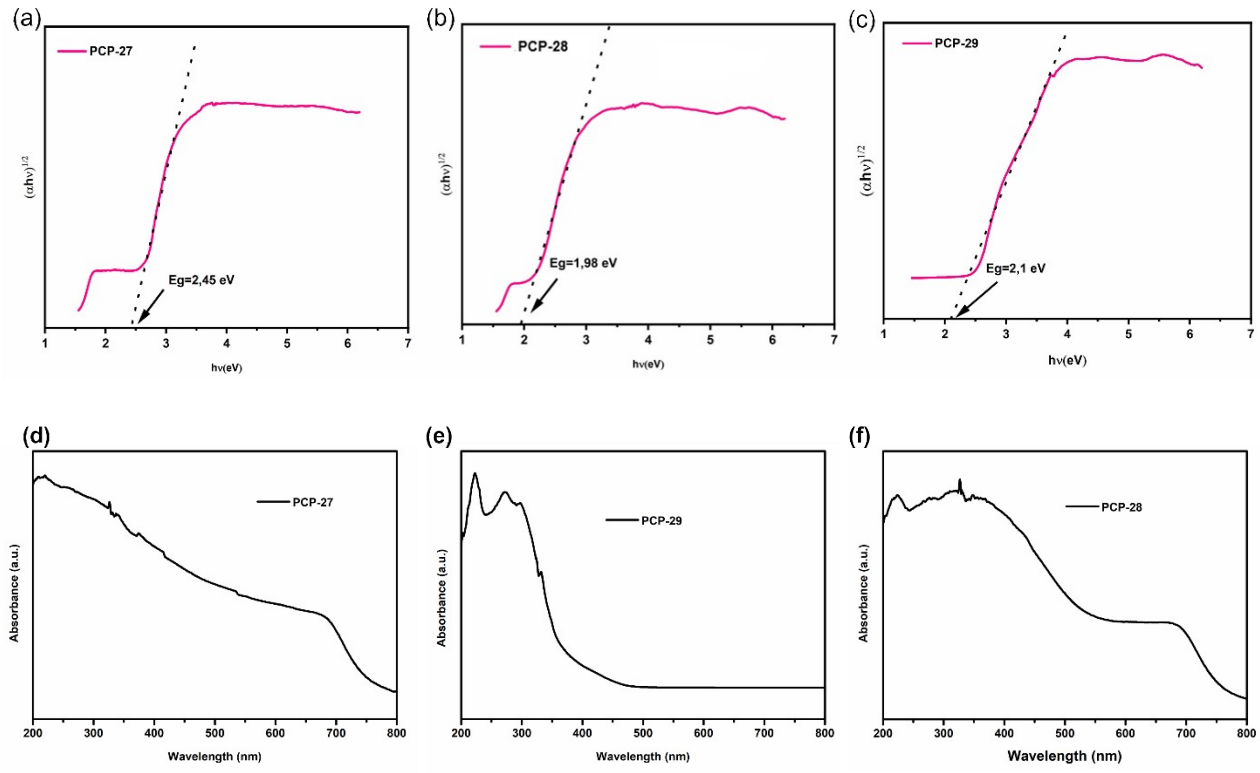

Figure S3. (a) Kubelka-Munk Plot of (a) **PCP-27** (b) **PCP-28** (c) **PCP-29.** UV-Vis absorption spectra of (d) **PCP-27** (e) **PCP-28** and (f) **PCP-29**.

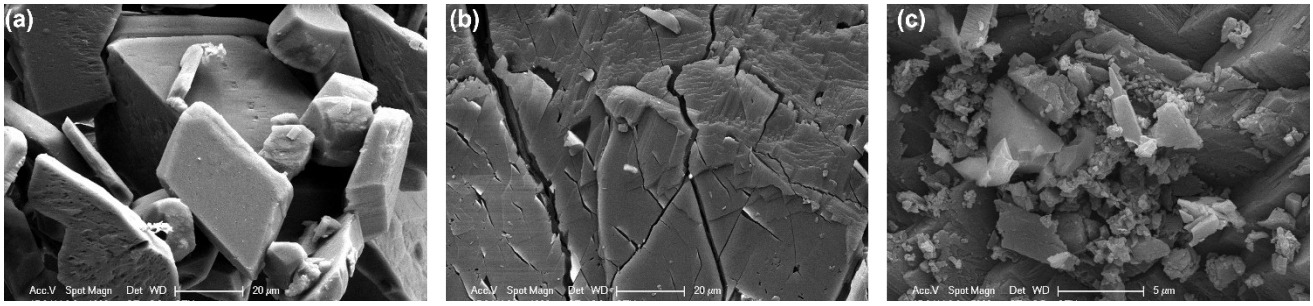

Figure S4. SEM images of (a) **PCP-27** (b) **PCP-28** (c) **PCP-29**.

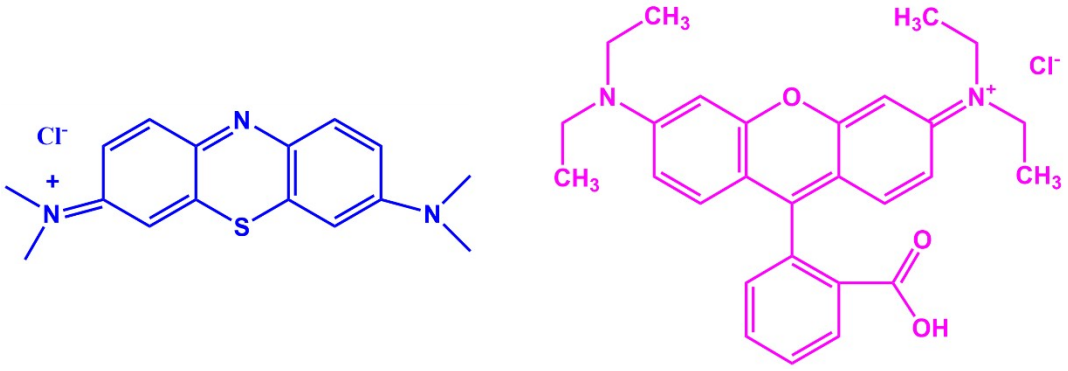

Methylene Blue (MB)
Cationic
λ_{max}= 665 nm
Mw= 319.85 g/mol

Rhodamine B (RhB)
Cationic
λ_{max}= 554 nm
Mw= 479.02 g/mol

Figure S5. Structure and properties of the model pollutants to be used in photocatalysis studies.

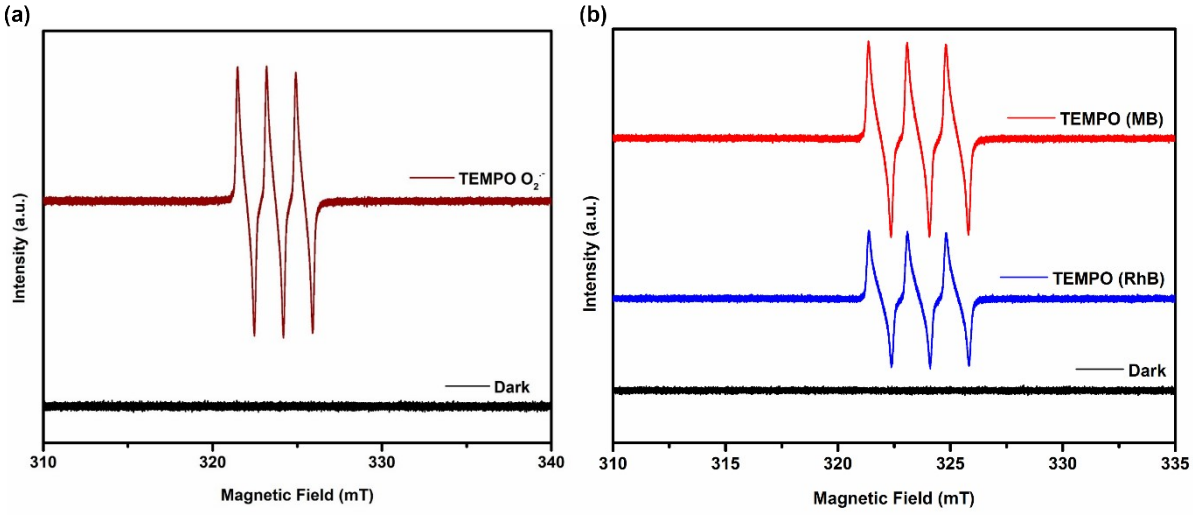

Figure S6. EPR detection of $O_2^{\bullet-}$ radical of **PCP-27** catalyst (a) and **PCP-29** (b).

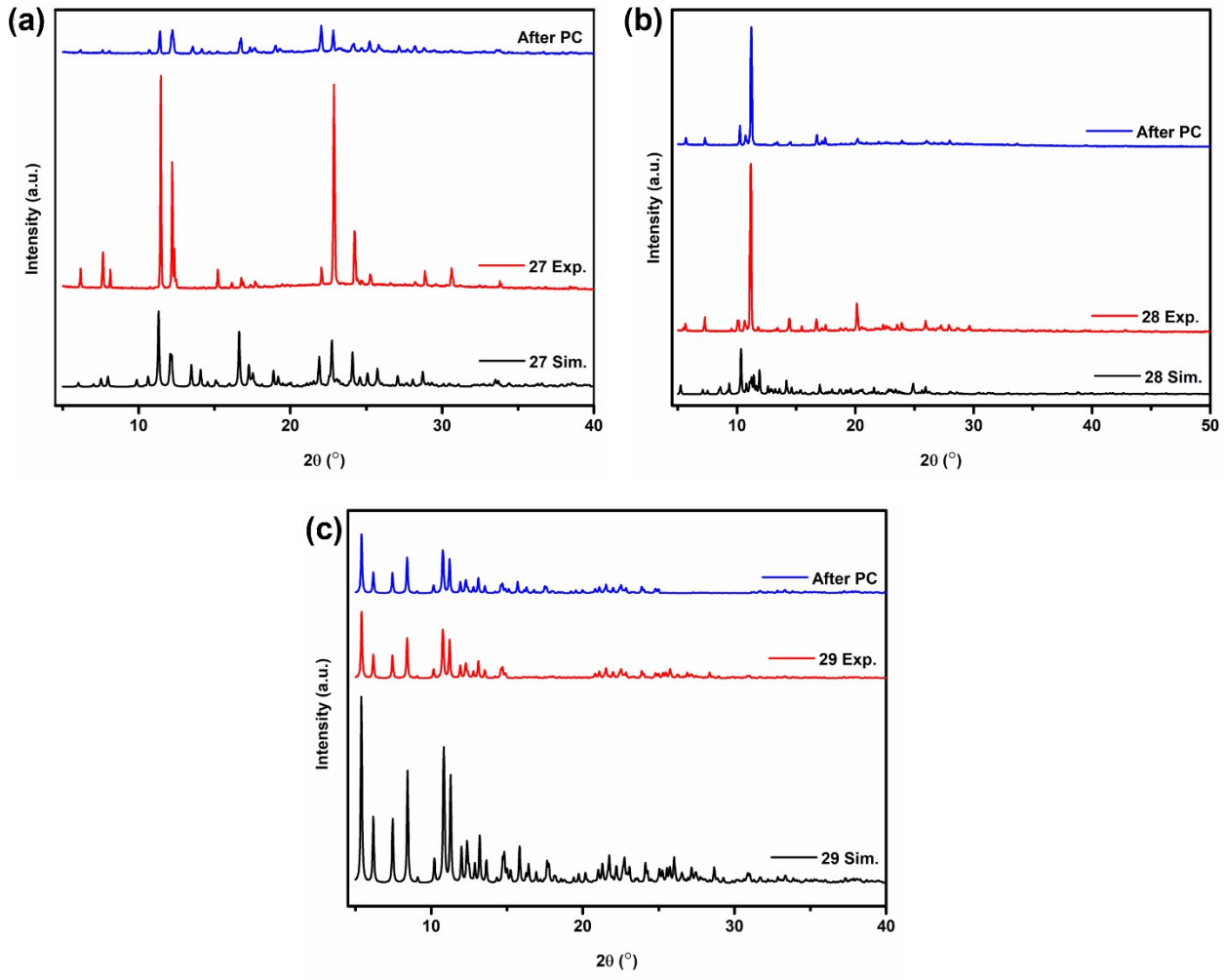

Figure S7. PXRD patterns of PCPs **27** (a), **28** (b), and **29** (c) showing simulated (black), experimental (red), and after photocatalysis (blue) results, confirming phase purity and structural stability.

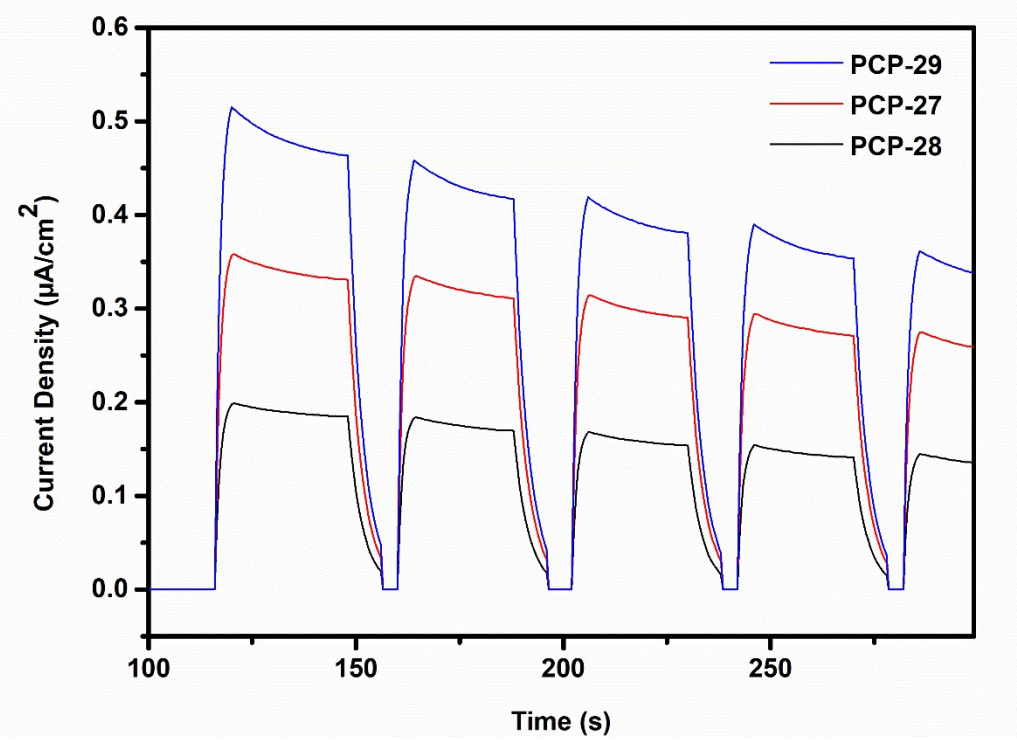

Figure S8. Transient photocurrent response of **PCP-27**, **PCP-28**, and **PCP-29** under periodic visible-light irradiation.

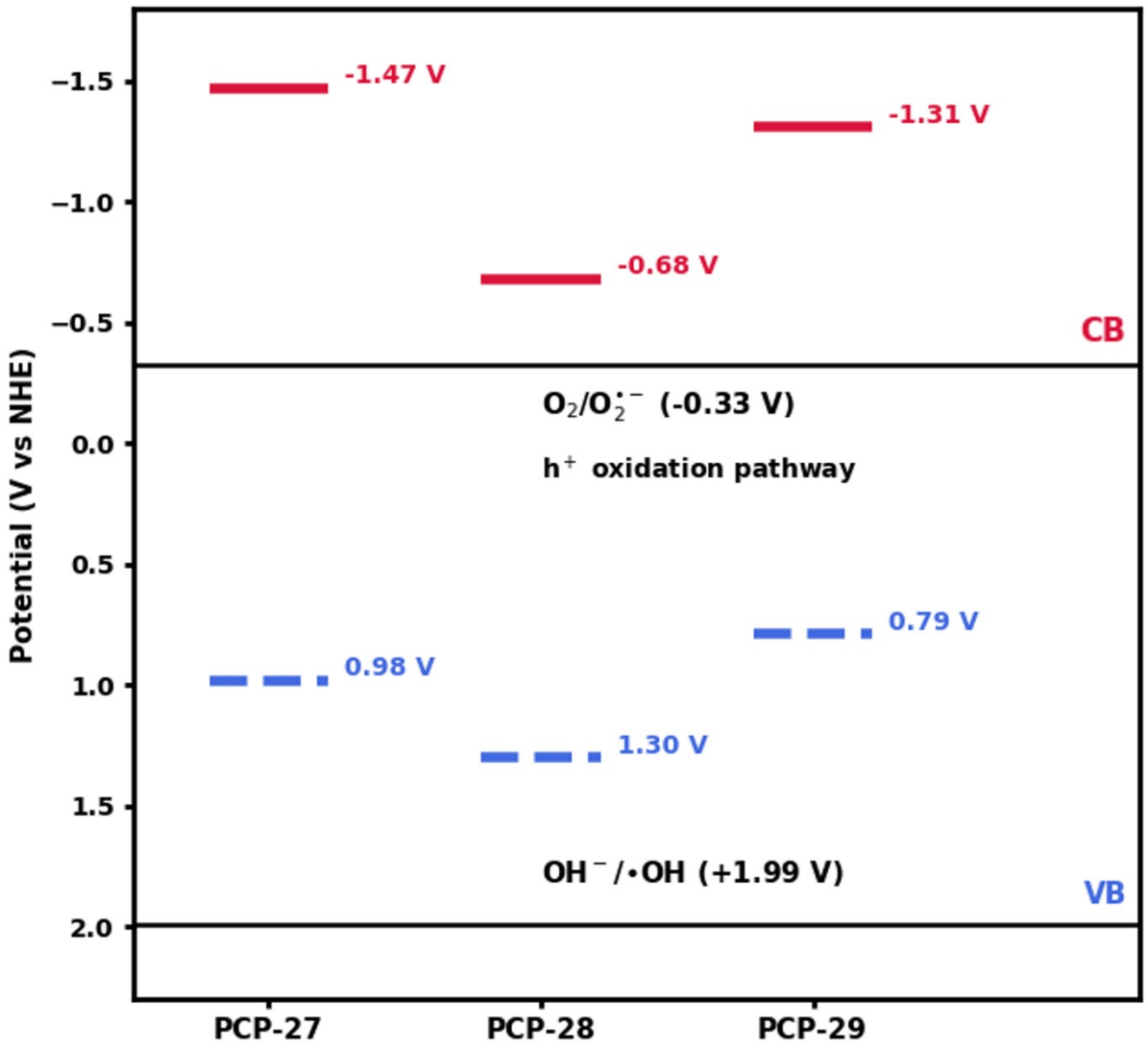

Figure S9. Schematic band alignment diagram of **PCP-27**, **PCP-28**, and **PCP-29** showing the calculated conduction band (CB) and valence band (VB) positions relative to the redox potentials of reactive oxygen species generation pathways, including $O_2/O_2^{\bullet-}$ (−0.33 V), $OH^-/^{\bullet}OH$ (+1.99 V), and hole (h^+) oxidation processes.

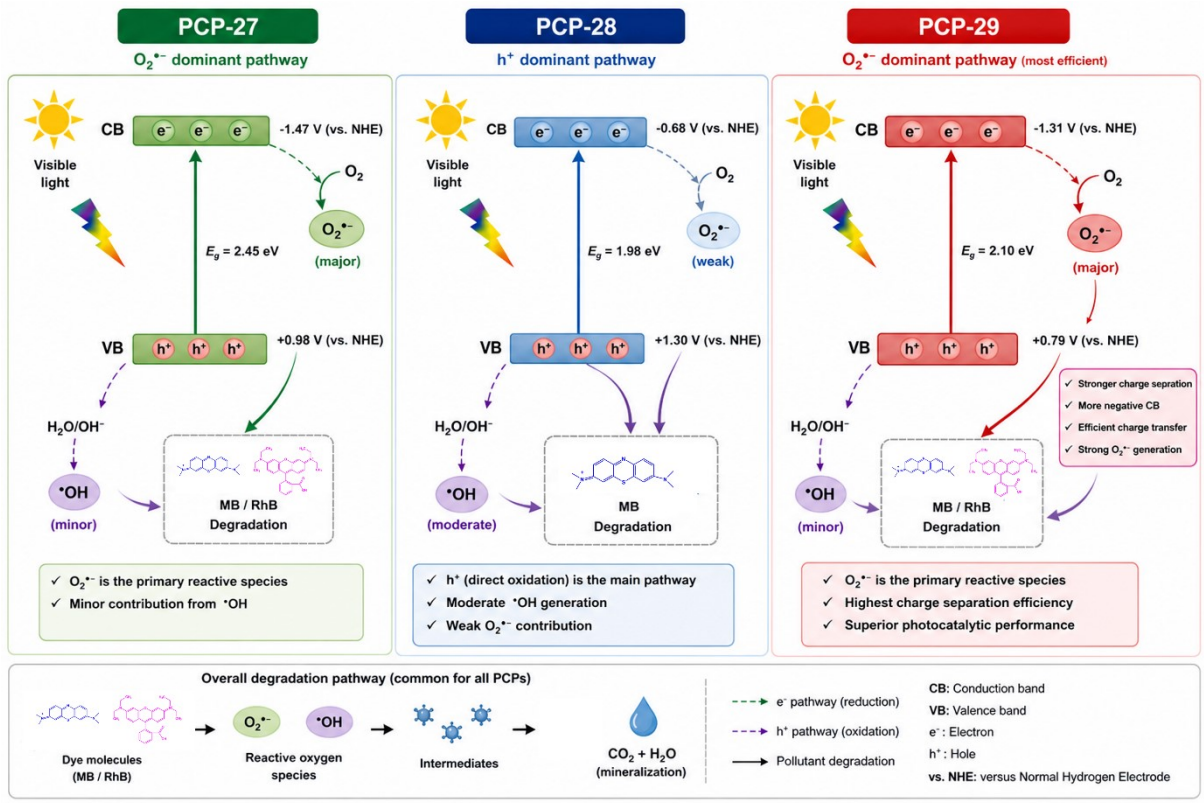

Figure S10. Comprehensive schematic illustration of the photocatalytic mechanisms of **PCP-27**, **PCP-28**, and **PCP-29** under visible-light irradiation, showing charge carrier generation, electron/hole migration pathways, band positions, dominant reactive oxygen species formation ($O_2^{\bullet-}$, $^{\bullet}OH$, and h^+), and the overall degradation pathway of dye molecules into final mineralization products.

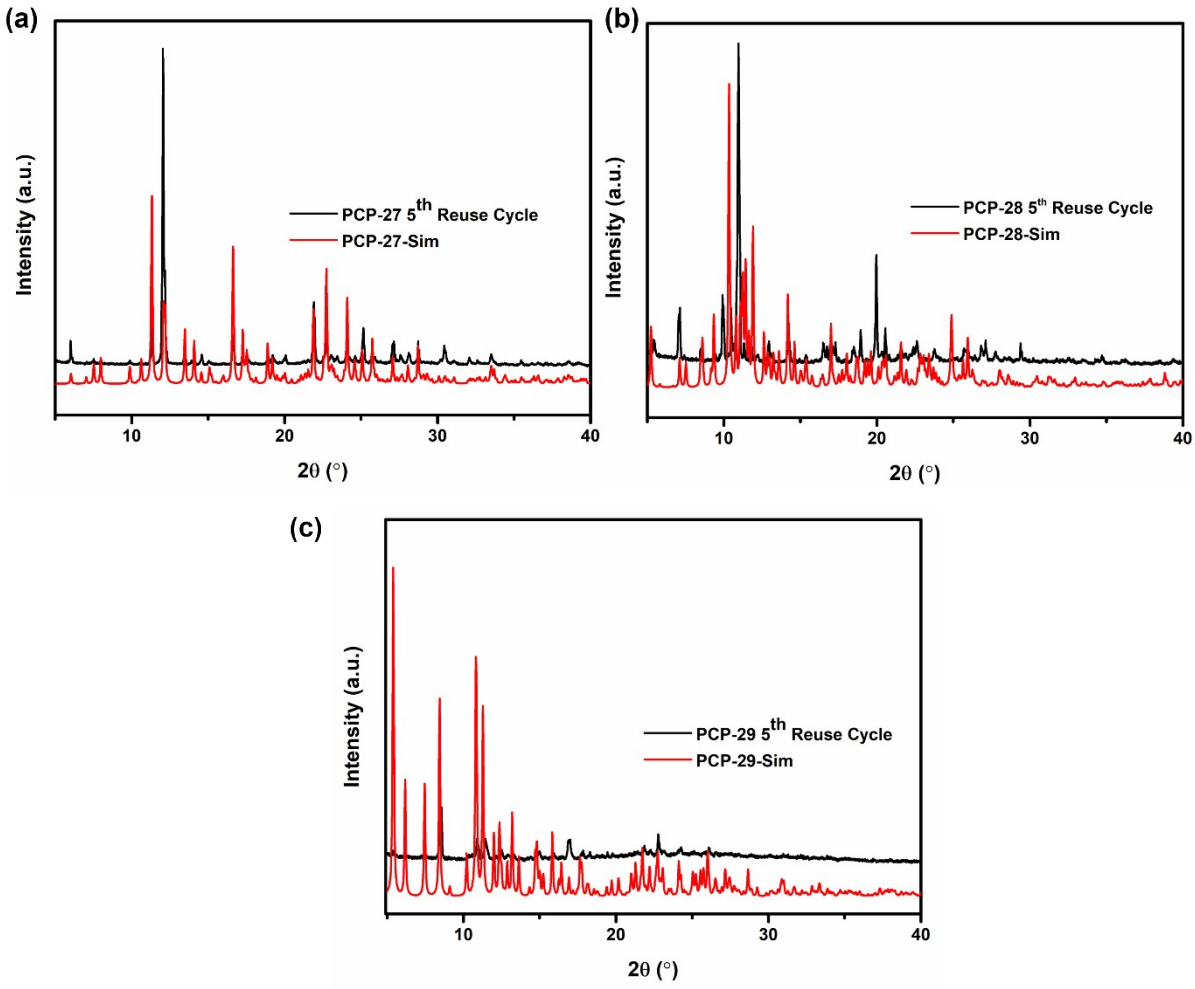

Figure S11. Post-catalytic PXRD patterns of recovered photocatalysts after five reuse cycles.

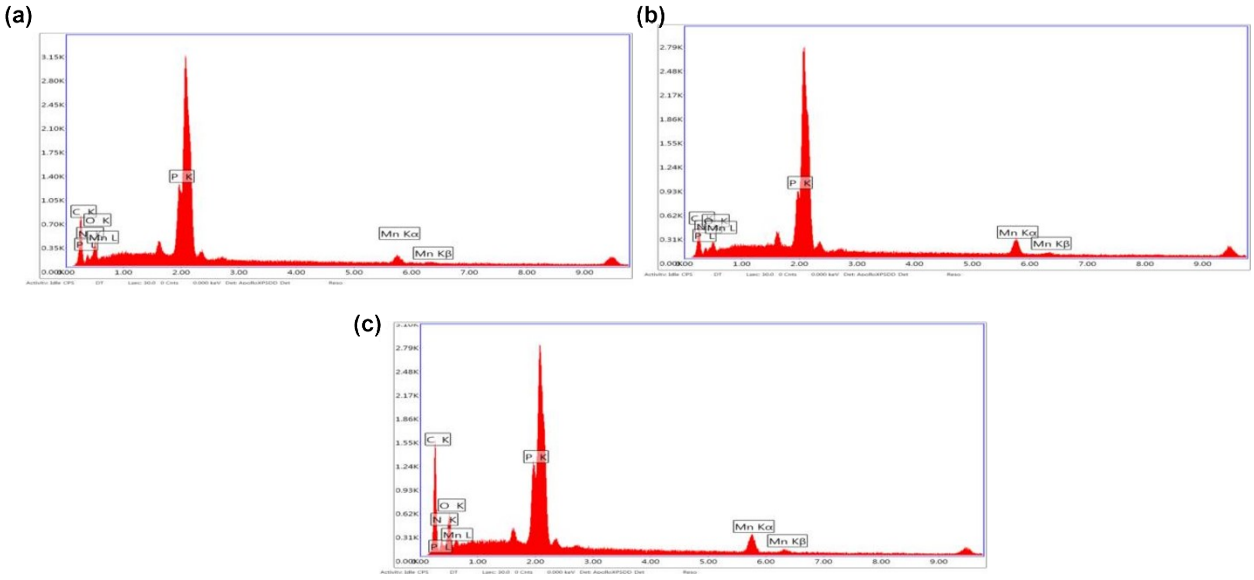

Figure S12. Post-catalytic EDX analysis of recovered photocatalysts after five reuse cycles.(a) **PCP-27** (b) **PCP-28** (c) **PCP-29.**

Table S1. Selected FT-IR spectral data for **H_4L** (cm^{-1}).

Ligand	$\upsilon_{(C-H)arom.}$	$\upsilon_{(C-H)alif}$	$\upsilon_{(C=O)}$	$\upsilon_{(P=N)}$	$\upsilon_{(P-O-C)}$	$\upsilon_{(C=C)}$	$\upsilon_{(O-H)}$
H_4L	3080	2827	1681	1263, 1158	1094	1504	3415

Table S2. Selected FT-IR spectral data for PCPs (cm^{-1}).

PCP	$\upsilon_{(C=O)}$	$\upsilon_{(P=N)}$	$\upsilon_{(C=C)}$	$\upsilon_{(C-H)arom.}$
PCP-27	υ_{as}1657 υ_s = 1340	1263, 1158	1511	3080
PCP-28	υ_{as}1605 υ_s = 1381	1262, 1152	1534	3085
PCP-29	υ_{as}1657 υ_s = 1381	1270, 1170	1552	3080

Table S3. The pseudo first-order rate constants k (min^{-1})and the corresponding square of the correlation coefficients R^2 data for the photocatalytic degradation reactions of MB and RhB catalyzed by PCPs.

	MB	**RhB**
PCP-27	0.02675 (0.96642)	0.01358 (0.95922)
PCP-28	0.00877 (0.97923)	-
PCP-29	0.0232 (0.93126)	0.02311 (0.94222)

Table S4. Photocatalytic removal performances of **PCP-27, PCP-28** and **PCP-29**.

PCPs	**MB**			**RhB**		
	Time (min)	**Dye Degradation %**	**5th Run %**	**Time (min)**	**Dye Degradation %**	**5th Run %**
PCP-27	90	90	55	90	75.444	66.40
PCP-28	90	59	40	90	-	-
PCP-29	90	91	70	90	91.723	70.15

Table S5. Elemental composition of **PCP-27**, **PCP-28**, and **PCP-29** obtained from EDX analysis after photocatalytic stability tests.

Element	PCP-27 (wt%)	PCP-27 (wt%)	PCP-28 (wt%)	PCP-28 (wt%)	PCP-29 (wt%)	PCP-29 (wt%)
C	45.40	60.60	37.80	56.97	47.81	62.37
N	10.16	11.63	10.37	13.40	11.05	12.36
O	14.02	14.05	8.48	9.59	14.94	14.63
P	21.42	11.09	22.61	13.21	14.36	7.27
Mn	8.99	2.62	20.74	6.83	11.84	3.38

Table S6. Crystallographic data and structure refinement details for PCPs.

Identification Code	PCP-27	PCP-28	PCP-29
Empirical formula	$C_{50}H_{34}MnN_5O_{14}P_3$	$C_{73}H_{57}Mn_2N_{10}O_{17}P_3$	$C_{67}H_{49}Mn_2N_8O_{16}P_3$
Formula weight	1076.67	1549.07	1424.93
Temperature/K	298	298	298
Crystal system	triclinic	triclinic	triclinic
Space group	P-1	P-1	P-1
a/Å	11.821(3)	13.670(3)	8.8654(17)
b/Å	13.087(4)	15.542(3)	17.045(4)
c/Å	15.171(5)	17.631(4)	21.439(4)
α/°	104.938(6)	78.702(5)	78.045(4)
β/°	91.171(6)	76.263(5)	84.341(4)
γ/°	95.993(6)	83.265(5)	78.032(4)
Volume/Å^3	2252.4(11)	3558.3(13)	3095.3(11)
Z	2	2	2
ρ_{calc}g/cm^3	1.587	1.446	1.529
μ/mm^{-1}	0.479	0.500	0.565
F(000)	1102.0	1592.0	1460.0
Crystal size/mm^3	0.23 × 0.12 × 0.05	0.32 × 0.14 × 0.11	0.28 × 0.22 × 0.12
Radiation	MoKα (λ = 0.71073)	MoKα (λ = 0.71073)	MoKα (λ = 0.71073)
2Θ range for data collection/°	3.242 to 50.348	2.414 to 50.28	3.44 to 50.202
Index ranges	-13 ≤ h ≤ 14, -15 ≤ k ≤ 15, -18 ≤ l ≤ 18	-16 ≤ h ≤ 16, -18 ≤ k ≤ 18, -21 ≤ l ≤ 21	-10 ≤ h ≤ 10, -20 ≤ k ≤ 20, -25 ≤ l ≤ 25
Reflections collected	22915	44553	29669
Independent reflections	8030 [R_{int} = 0.0664, R_{sigma} = 0.0907]	12605 [R_{int} = 0.0863, R_{sigma} = 0.1016]	10964 [R_{int} = 0.0832, R_{sigma} = 0.1302]
Data/restraints/parameters	8030/1/662	12605/642/883	10964/0/811
Goodness-of-fit on F^2	0.995	1.058	0.930
Final R indexes [I>=2σ (I)]	R_1 = 0.0517, wR_2 = 0.1130	R_1 = 0.0838, wR_2 = 0.2374	R_1 = 0.0529, wR_2 = 0.1101
Final R indexes [all data]	R_1 = 0.1056, wR_2 = 0.1355	R_1 = 0.1350, wR_2 = 0.2685	R_1 = 0.1094, wR_2 = 0.1309
Largest diff. peak/hole / e Å^{-3}	0.52/-0.56	0.57/-0.50	0.29/-0.40

Table S7. Selected bond lengths (Å) and bond angles (°) for **PCP-27.**

Bond Lengths (Å)			
Mn1—O2^i	2.323 (3)	P1—N2	1.578 (3)

Mn1—O4^{i}	2.075 (3)	P1—N1	1.583 (3)
Mn1—O13	2.061 (3)	P3—N3	1.571 (3)
Mn1—N4	2.272 (3)	P2—N1	1.571 (3)
Mn1—N5	2.256 (3)	P2—N3	1.579 (3)
		P3—N2	1.570 (3)
Bond Angles (°)			
O4^{i}—Mn1—O2^{i}	80.61 (12)	O4^{i}—Mn1—O2^{i}	80.61 (12)
O4^{i}—Mn1—N4	83.90 (12)	O4^{i}—Mn1—N4	83.90 (12)
O4^{i}—Mn1—N5	147.19 (12)	O4^{i}—Mn1—N5	147.19 (12)
O13—Mn1—O2^{i}	91.22 (11)	O13—Mn1—O2^{i}	91.22 (11)
O13—Mn1—O4^{i}	127.42 (11)	O13—Mn1—O4^{i}	127.42 (11)
O13—Mn1—N4	139.74 (12)	O13—Mn1—N4	139.74 (12)
O13—Mn1—N5	84.86 (11)	O13—Mn1—N5	84.86 (11)
N4—Mn1—O2^{i}	121.61 (11)	N4—Mn1—O2^{i}	121.61 (11)
N5—Mn1—O2^{i}	94.62 (12)	P3—N3—P2	121.5 (2)
N5—Mn1—O2^{i}	94.62 (12)	P2—N1—P1	123.47 (18)
N5—Mn1—N4	70.98 (12)	P3—N2—P1	122.7 (2)
N2—P3—N3	118.09 (16)	P3—N2—P1	122.7 (2)
N1—P2—N3	117.23 (17)	N2—P1—N1	116.15 (16)

Symmetry codes: (i) x, y+1, z+1.

Table S8. Selected bond lengths (Å) and bond angles (°) for **PCP-28.**

Bond Lengths (Å)			
Mn1—O1	2.034 (5)	Mn2—N5	2.252 (6)
Mn1—O7^{i}	2.077 (6)	Mn2—N6	2.252 (6)
Mn1—N1	2.274 (6)	Mn2—N4	2.340 (6)
Mn1—N2	2.216 (5)	P3—N7	1.586 (5)
Mn1—N3	2.252 (7)	P3—N8	1.569 (5)
Mn2—O3	2.489 (6)	P1—N7	1.568 (5)
Mn2—O4	2.169 (5)	P1—N9	1.572 (5)
Mn2—O5^{i}	2.415 (5)	P2—N8	1.578 (5)
Mn2—O6^{i}	2.219 (5)	P2—N9	1.585 (5)
Bond Angles (°)			
O1—Mn1—O7^{i}	105.2 (2)	O4—Mn2—O3	55.5 (2)
O1—Mn1—N1	87.0 (2)	O4—Mn2—O5^{i}	83.19 (19)
O1—Mn1—N2	109.3 (2)	O4—Mn2—O6^{i}	105.2 (2)
O1—Mn1—N3	105.5 (3)	O4—Mn2—N4	84.7 (2)
O7^{i}—Mn1—N1	102.4 (2)	O4—Mn2—N5	146.0 (2)
O7^{i}—Mn1—N2	144.6 (2)	O4—Mn2—N6	123.7 (2)
O7^{i}—Mn1—N3	107.4 (3)	O5^{i}—Mn2—O3	116.52 (18)
N2—Mn1—N1	71.8 (2)	O6^{i}—Mn2—O3	160.8 (2)
N2—Mn1—N3	71.2 (2)	O6^{i}—Mn2—O5^{i}	55.94 (17)
N3—Mn1—N1	143.0 (2)	O6^{i}—Mn2—N4	84.7 (2)
O6^{i}—Mn2—N5	94.9 (2)	N6—Mn2—N4	139.6 (2)
O6^{i}—Mn2—N6	110.4 (2)	N5—Mn2—O3	101.79 (19)
N5—Mn2—N4	69.9 (2)	N7—P1—N9	118.3 (3)
N5—Mn2—N6	71.5 (2)	N8—P3—N7	117.4 (3)
N6—Mn2—O3	84.2 (2)	P1—N7—P3	120.4 (3)
N6—Mn2—O5^{i}	82.3 (2)	P3—N8—P2	122.1 (3)
N4—Mn2—O3	92.1 (2)	P1—N9—P2	121.3 (3)
N4—Mn2—O5^{i}	133.39 (19)	N8—P2—N9	117.7 (3)

N5—Mn2—O5^{i}	130.76 (19)		

Symmetry codes: (i) *x*, *y*−1, *z*; (ii) *x*, *y*+1, *z*.

Table S9. Selected bond lengths (Å) and bond angles (°) for **PCP-29.**

Bond Lengths (Å)			
Mn1—O7^{i}	2.303 (3)	Mn2—N7	2.252 (4)
Mn1—O9^{i}	2.128 (3)	Mn2—N6	2.236 (4)
Mn1—O12^{ii}	2.229 (3)	Mn2—O12^{iii}	2.344 (3)
Mn1—O13	2.107 (3)	P1—N1	1.577 (3)
Mn1—N4	2.262 (3)	P1—N3	1.578 (3)
Mn1—N5	2.265 (3)	P3—N3	1.566 (3)
Mn2—O8	2.109 (3)	P3—N2	1.593 (3)
Mn2—O10	2.098 (3)	P2—N1	1.577 (3)
Mn2—O11^{iii}	2.279 (3)	P2—N2	1.572 (3)
Bond Angles (°)			
O9^{i}—Mn1—O7^{i}	80.06 (11)	O10—Mn2—O12^{iii}	99.50 (11)
O9^{i}—Mn1—O12^{ii}	102.68 (11)	O10—Mn2—N6	95.51 (13)
O9^{i}—Mn1—N4	94.44 (13)	O10—Mn2—N7	167.43 (13)
O9^{i}—Mn1—N5	166.47 (11)	O11^{iii}—Mn2—O12^{iii}	56.77 (9)
O12^{ii}—Mn1—O7^{i}	87.42 (11)	N7—Mn2—O12^{iii}	92.87 (11)
O12^{ii}—Mn1—N4	160.26 (12)	N6—Mn2—O11^{iii}	85.11 (11)
O12^{ii}—Mn1—N5	88.86 (11)	N6—Mn2—O12^{iii}	138.53 (10)
O13—Mn1—O7^{i}	165.14 (12)	N6—Mn2—N7	73.49 (13)
O13—Mn1—O9^{i}	86.74 (12)	N7—Mn2—O11^{iii}	95.38 (11)
O13—Mn1—O12^{ii}	88.87 (10)	O10—Mn2—O8	88.69 (12)
O13—Mn1—N4	101.97 (12)	O10—Mn2—O11^{iii}	89.60 (11)
O13—Mn1—N5	100.70 (12)	O8—Mn2—N7	87.19 (12)
N4—Mn1—O7^{i}	85.94 (12)	N1—P1—N3	117.20 (17)
N4—Mn1—N5	73.06 (12)	N2—P2—N1	118.06 (18)
N5—Mn1—O7^{i}	93.61 (11)	P2—N1—P1	122.0 (2)
O8—Mn2—O11^{iii}	175.27 (12)	P2—N2—P3	122.1 (2)
O8—Mn2—O12^{iii}	119.23 (12)	P3—N3—P1	122.8 (2)
O8—Mn2—N6	99.44 (13)	N3—P3—N2	116.51 (18)

Symmetry codes: (i) *x*−1, *y*+1, *z*; (ii) *x*−1, *y*, *z*; (iii) *x*, *y*−1, *z*; (iv) *x*+1, *y*−1, *z*; (v) *x*, *y*+1, *z*; (vi) *x*+1, *y*, *z*.

Table S10. Comparison of photocatalytic activity of Mn(II) PCPs from literature and PCPs synthesized in this study.

Coordination Polymers	**Dye**	**Light Source**	**Time (min)**	**% Degradation**	**Ref.**
$[Mn(cpip)(NO_2\text{-}bdc)]_n \cdot 0.5H_2O$ (2)	CR	Visible light (λ > 420 nm)	120	95.84	[1]
$[Mn(cpip)(NO_2\text{-}bdc)]_n \cdot 0.5H_2O$ (2)	MV	Visible light (λ > 420 nm)	120	90.32	[1]
$[Mn(cpip)(NO_2\text{-}bdc)]_n \cdot 0.5H_2O$ (2)	MB	Visible light (λ > 420 nm)	120	84.87	[1]
$[Mn_2(cpip)_2(HO\text{-}bdc)]$n (1)	CR	Visible light (λ > 420 nm)	120	69.24	[1]
$[Mn_2(cpip)_2(HO\text{-}bdc)]$n (1)	MV	Visible light (λ > 420 nm)	120	35.18	[1]
$[Mn_2(cpip)_2(HO\text{-}bdc)]$n (1)	MB	Visible light (λ > 420 nm)	120	54.56	[1]
$\{Mn(bimb)(2,6\text{-}NDA)\}_n$ (Mn-MOF)	MB	White light (Xe lamp)	480	99.55	[2]

$[Mn_2(L)(bpy)(H_2O)_2.2H_2O]_n$	MV	UV	50	93.1	[3]
Mn-MOF	MB	Visible light (Xe lamp)	63	60	[4]
Mn-MOF + H_2O_2	MB	Visible light (Xe lamp)	25	90	[4]
$[Mn(SCN)_2(peol)]_n$ (1D CP)	Alizarin	Not specified	50	86.12	[5]
$[Mn_2L(1,10\text{-phen})_2]DMF.0.5H_2O$ (1)	RhB	UV Light	56.27	8 h	[6]
$[Mn(1,10\text{-phen})(SO_4)\ (H_2O)_2]$ (2)	RhB	UV Light	32.46	8 h	[6]
PCP-28	MB	Visible	90	68	**This Study**
PCP-29	MB	Visible	90	92	**This Study**
PCP-27	RhB	Visible	90	75.44	**This Study**
PCP-28	RhB	Visible	90	-	**This Study**
PCP-29	RhB	Visible	90	91.72	**This Study**

Hcpip : 2-(2-carboxyphenyl) imidazo(4,5-f)-(1,10)phenanthroline; bimb: 1,4-bis[(1H-imidazol-1-yl)methyl] benzene; 2,6-NDA: 2,6-naphthalenedicarboxylic acid); H_4L : bis-(3,5-dicarboxypheny1) terephthalamide; H_2L : 2,2′-bipyridine-4,4′-dicarboxylic acid.

References

[1] C. Sun, J. Jian, N. Lv, X. Xue, J. Shi, T. Zhou, L. Zhao, Y. Qiao, G. Che, "Synthesis, characterization, selective degradation of organic dyes and mechanism study of two novel Mn(II)-based coordination polymers" *J. Mol. Struct.* **2025**, *1327*, 141114.

[2] K. Li, S. J. Li, W. J. Shi, X. Y. Zhang, Y. L. Li, "Enhanced photocatalytic degradation of MB dye by Mn/Co-MOFs with mixed ligands" *J. Mol. Struct.* **2026**, *1366*, 145955.

[3] Y. Wu, M. K. Ghosh, Y. Lv, X. Hou, X. Wang, J. Wang, T. K. Ghorai, M. Muddassir, J. Guo, "Synthesis and characterization Mn(II) and Co(II) based coordination polymer and photocatalytic activity against methyl violet" *Polyhedron* **2023**, *243*, 116575.

[4] S. T. Karunakaran, R. Pavithran, M. Sajeev, S. M. M. Rema, "Photocatalytic degradation of methylene blue using a manganese based metal organic framework" *Results Chem.* **2022**, *4*, 100504.

[5] J. Du, X. Yang, F. Yuan, "A new Mn(II) coordination polymer and its application in the degradation of alizarin" *J. Coord. Chem.* **2024**, *77*, 983–990.

[6] F. Wang, C. Wang, Z. Yu, K. Xu, X. Li, Y. Fu, "Two multifunctional Mn(II) metal-organic frameworks: Synthesis, structures and applications as photocatalysis and luminescent sensor" *Polyhedron* **2016**, *105*, 49–55.